

Gravitational lensing by wave dark matter halos

Antonio Herrera-Martín,^{1,*} Martin Hendry,^{1,†} Alma X. Gonzalez-Morales,^{2,3,‡} and L. Arturo Ureña-López^{3,§}

¹*SUPA, University of Glasgow, Glasgow, G12 8QQ, United Kingdom*

²*Consejo Nacional de Ciencia y Tecnología, Av. Insurgentes Sur 1582. Colonia Crédito Constructor, Del. Benito Juárez C.P. 03940, México D.F. México*

³*Departamento de Física, DCI, Campus León, Universidad de Guanajuato, 37150, León, Guanajuato, México.*

(Dated: August 1, 2017)

Wave Dark Matter (WaveDM) has recently gained attention as a viable candidate to account for the dark matter content of the Universe. In this paper we explore the extent to which dark matter halos in this model, and under what conditions, are able to reproduce strong lensing systems. First, we analytically explore the lensing properties of the model – finding that a pure WaveDM density profile, a soliton profile, produces a weaker lensing effect than other similar cored profiles. Then we analyze models with a soliton embedded in an NFW profile, as has been found in numerical simulations of structure formation. We use a benchmark model with a boson mass of $m_a = 10^{-22}$ eV, for which we see that there is a bi-modality in the contribution of the external NFW part of the profile, and actually some of the free parameters associated with it are not well constrained. We find that for configurations with boson masses $10^{-23} - 10^{-22}$ eV, a range of masses preferred by dwarf galaxy kinematics, the soliton profile alone can fit the data but its size is incompatible with the luminous extent of the lens galaxies. Likewise, boson masses of the order of 10^{-21} eV, which would be consistent with Lyman- α constraints and consist of more compact soliton configurations, necessarily require the NFW part in order to reproduce the observed Einstein radii. We then conclude that lens systems impose a conservative lower bound $m_a > 10^{-24}$ and that the NFW envelope around the soliton must be present to satisfy the observational requirements.

I. INTRODUCTION

The Λ CDM model is the most successful theoretical framework in modern cosmology to explain the process of structure formation in the Universe on large scales. This model requires the existence of a cold dark matter (CDM) component that comprises 26% of the total energy budget, which is best described by a non-relativistic (cold) and non-interacting fluid [1].

One of the main predictions from only CDM simulations of structure formation is the appearance of universal cuspy density profiles for the DM halos, with the Navarro, Frenk and White (NFW) profile the one most used to describe CDM [2]. Despite the successes of CDM at large scales, there are some discrepancies with observations on galactic scales, such as: the “missing satellite problem”, the “cusp core problem”, and the “too-big-to-fail problem” [3–9], see also Ref.[10] for a recent review. Solutions to these problems may come from taking into account the effects of baryons in the formation of galaxies, but it is doubtful that this is the final answer. Another possibility to solve the above mentioned issues is to change the paradigm of the nature of dark matter itself, as has been proposed and explored widely for different candidates such as Self-Interacting Dark Matter [11], Warm Dark Matter [12, 13], Axion/Scalar or Wave Dark Matter [14–19], and other specifications of the nature of

dark matter particles, which can actually be described in a more general effective theory [20].

In this paper, our approach is to describe the dark matter as an axion/scalar field that we will refer to here as a Wave Dark Matter model (WaveDM, also referred sometimes to as scalar field DM, ultralight axion-like DM, fuzzy DM, etc.). This type of model has been worked out by several other authors [14–18], and has been found to be able to reproduce the success of the Λ CDM model on cosmological scales, but it predicts a natural cut-off on the mass power spectrum of linear perturbations that helps to alleviate most of the low-scale issues of CDM [15, 17, 21, 22]. Interestingly enough, all cosmological effects are directly related to a single parameter, which is the boson mass of the scalar field particle m_a (although extra observational effects may arise from quartic self-interactions[23–26]). Based on considering the cut-off of the mass power spectrum, the halo mass function, the reionization time or the Lyman- α forest, the most up-to-date constraints suggest that the boson mass must satisfy $m_a > 1 \times 10^{-21}$ eV [27, 28].

However, the non-linear process of structure formation under the SFDM hypothesis does not depend on a single parameter only, but rather one requires to take into account at least one second parameter. This fact is indeed considered in many recent studies that try to put constraints on the SFDM parameters with data coming from, for instance, satellite galaxies in the Milky Way[19, 29–32]. The aforementioned studies consider that galaxies are described by a solitonic core with a negligible self-interaction, known as ψ DM, or WaveDM. The soliton solution is just the ground state of the so-called Schrodinger-Poisson system of equations[33, 34], and its

* a.herrera-martin.1@research.gla.ac.uk

† martin.hendry@glasgow.ac.uk

‡ alma.gonzalez@fisica.ugto.mx

§ lurena@ugto.mx

wave-like properties provide stability against gravitational collapse – opening the possibility of naturally-supported, cored halos. The full prescription of the WaveDM profile requires specification of the boson mass m_a together with one of its structure parameters, which can be taken to be either the central density or the scale radius, while the other is determined by the relation,

$$\frac{\rho_s}{M_\odot \text{pc}^{-3}} = 2.4 \times 10^{12} \left(\frac{r_s}{\text{pc}} \right)^{-4} \left(\frac{m_a}{10^{-22} \text{eV}} \right)^{-2}. \quad (1)$$

The boson mass m_a is expected to be a fundamental parameter with a single value for all galaxies, while the other two parameters may take values that differ from galaxy to galaxy. All of the above strongly indicates that we require to think more carefully if we are to obtain meaningful constraints on the boson mass. More specifically, if we consider the boson mass as an universal parameter, on the same footing as any other cosmological parameter, we should certainly be able to use statistical analysis of galaxy data to constrain which values are permitted, as has been proposed to do in [35, 36] and more recently done in [30, 31]. However, in general, we may be unable to assert whether there is one single value of m_a that is suitable to satisfy all the possible constraints.

It has been shown that the NFW profile correctly describes the observed lensing signal in a large sample of systems, in particular in the SLACS survey [37]. However, since the wave dark matter is considered a feasible candidate for DM, in this work we study the behaviour of, and constraints upon, a WaveDM type of profile acting as a gravitational lens, and we obtain the conditions under which the profile will be able to produce strong lensing.

A brief description of the paper is as follows. The basic lensing equations for any given density profile are described in Sec. II, where we also introduce the explicit lensing expressions for the particular case of the WaveDM profile. In Sec. III we describe our statistical analysis and present the results arising from the comparison of the WaveDM model predictions with selected data from the SLACS catalog. Finally, the general conclusions are presented in Sec. IV. Some analytical solutions of the lens equations used in the text are presented in the appendix.

II. GRAVITATIONAL LENSING WITH A ψ DM PROFILE

A. General lensing equations

One of the main predictions from Einstein's General Relativity (GR) is the bending of light as it passes close to a massive body. The deflection angle produced by this effect depends on the mass of the deflector, acting like a lens. This deflector may be approximated by a point-like mass, such as a star, but for more massive objects like galaxies it is better to represent them as extended masses which are described by their density profiles.

The simplest type of lens is a system with a point mass M located close to the line of sight to a luminous source S . Due to the gravitational field of the point mass, a light ray is deflected in its path to the observer; this is described by the Lens Equation in the thin lens approximation. The same approximation also holds for a mass distribution, in which case the lens equation is [38],

$$\beta = \theta - \frac{m(\theta)}{\pi \Sigma_{cr} D_{OL}^2 \theta}, \quad (2)$$

that relates the (unobservable) angle between, the line of sight and the path from the observer to actual position of the source, β , and to the apparent position of the source (the image), θ , to the mass distribution that is causing the lensing $m(\xi)$. Here we have assumed that $m(\xi)$ is the projected mass enclosed in a circle of radius $\xi \equiv D_{OL}\theta$; more explicitly, we can write

$$m(\xi) = 2\pi \int_0^\xi d\hat{\xi} \hat{\xi} \Sigma(\hat{\xi}). \quad (3a)$$

The projected surface mass density $\Sigma(\xi)$ can be calculated directly from the (spherically symmetric) density profile $\rho(r)$ of the lensing object as:

$$\Sigma(\xi) = 2 \int_0^{z_{\max}} dz \rho(z, \xi), \quad (3b)$$

where $z \equiv \sqrt{r^2 - \xi^2}$ is a coordinate in the direction orthogonal to the line of sight, so that $0 \leq \xi \leq r$. If the lens system has a finite radius r_{\max} , then $z_{\max} = \sqrt{r_{\max}^2 - \xi^2}$; otherwise, we can put $z_{\max} \rightarrow \infty$ in the integral (3b).

Let us consider the case in which the density profile ρ has a characteristic density ρ_s , and a characteristic radius r_s , such that $\rho(r) = \rho_s f(r/r_s)$ where f is the function that accounts for the shape of the profile. We can then write Eq. (2) in the dimensionless form

$$\beta_*(\theta_*) = \theta_* - \lambda \frac{m_*(\theta_*)}{\theta_*}, \quad (4)$$

where the different distances are normalized in terms of r_s : $\beta_* = D_{OL}\beta/r_s$, $\theta_* = D_{OL}\theta/r_s$, and then $\xi_* = \xi/r_s = \theta_*$. The latter equation means that the normalized variables ξ_* and θ_* can be used interchangeably, and then hereafter we will use θ_* as our distance variable. Likewise, the total mass, as given in Eq. (3a), is normalized as

$$m_*(\theta_*) = \frac{m(\theta_*)}{\rho_s r_s^3} = 2\pi \int_0^{\theta_*} d\hat{\theta}_* \hat{\theta}_* \Sigma_*(\hat{\theta}_*), \quad (5a)$$

where the normalized projected surface mass density, from Eq. (3b), is

$$\Sigma_*(\theta_*) = \frac{\Sigma(\theta_*)}{\rho_s r_s} = 2 \int_0^{z_{\max}^*} dz f(z, \theta_*), \quad (5b)$$

with $z = \sqrt{r_*^2 - \theta_*^2}$ and $r_* = r/r_s$. The new parameter λ in Eq. (4) is then given by

$$\lambda \equiv \frac{\rho_s r_s}{\pi \Sigma_{\text{cr}}} = 10^{-3} \frac{0.57}{h} \left(\frac{\rho_s r_s}{M_{\odot} \text{pc}^{-2}} \right) \frac{d_{\text{OL}} d_{\text{LS}}}{d_{\text{OS}}} \quad (6)$$

Equation (6) contains information about the lensing properties of any given model, together with that of the different distances involved in the lens system.¹

One particular case of interest is that of perfect alignment between the luminous source and the lens system for which $\beta_*(\theta_{*E}) = 0$. This in turn defines an Einstein ring with radius $R_E = D_{\text{OL}} \theta_E$ with an associated angular radius θ_E . In terms of our normalized variables, we see that that the observed Einstein radius is just $R_E/r_s = \theta_{*E}$. In other words, the normalized angular Einstein radius θ_{*E} directly is the ratio of the Einstein radius to the scale radius of the density profile. Moreover, the angular radius θ_{*E} must also be a solution of the equation [see Eq. (4)]

$$\lambda = \frac{\theta_{*E}^2}{m_*(\theta_{*E})}. \quad (7)$$

Interestingly enough, Eq. (7) shows that the lensing properties of a system with a density profile of the form $\rho(r) = \rho_s f(r/r_s)$ are independent of the density and distance scales, and are mostly sensitive to the particular shape of the density profile. The physical parameters of the system are then concentrated in the dimensionless parameter λ in Eq. (6), and the latter can be calculated from Eq. (7) without any prior knowledge of the given physical scales in the system, namely ρ_s and r_s , under the only assumption of perfect alignment (see Fig. 1 below for an example).

There is a critical value λ_{cr} that is the smallest value of λ for which an Einstein ring appears, which must correspond to the limit $\theta_{*E} \rightarrow 0$ in Eq. (7). As we shall show now, such a critical value can be calculated analytically in the general case. To avoid the divergence at $\theta_{*E} = 0$ (where $m_*(0) = 0$), we make use of the L'Hôpital rule in Eq. (7), and from Eq. (3a) we finally obtain

$$\lambda_{\text{cr}}^{-1} = \pi \Sigma_*(0) = 2\pi \int_0^{r_{\text{max}^*}} d\hat{r}_* f(\hat{r}_*), \quad (8)$$

where $\Sigma(0)$ is the central value of the projected surface mass density given by Eq. (3b). Eq. (8) is quite a simple formula for the calculation of λ_{cr} for any given density profile $\rho(r)$.²

As said before, Eq. (8) suggests that the critical value λ_{cr} just depends on the particular shape of the given

Name	Density profile $f(r)$	λ_{cr}
NFW [40]	$[(r/r_s)(1+r/r_s)^2]^{-1}$	0
Burkert [39]	$[(1+r/r_s)(1+r^2/r_s^2)]$	$2/\pi^2 \simeq 0.203$
SFDM [35]	$\sin(\pi r/r_s)/(\pi r/r_s)$	0.27
WaveDM	$(1+r^2/r_s^2)^{-8}$	$\frac{2048}{429\pi^2} \simeq 0.484$

TABLE I. The intrinsic value λ_{cr} , calculated from Eq. (8), for dark matter halos with different density profiles. This critical value is the minimum value of λ in Eq. (7) for which the lens system will produce multiple images, i.e. an Einstein ring.

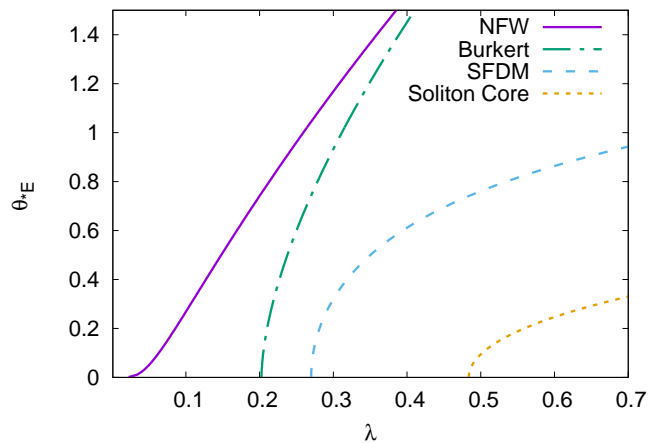


FIG. 1. The Einstein radius θ_{*E} as a function of λ for different individual profiles, see Eq. (7). The point where each curve crosses the horizontal axis indicates the (intrinsic) critical value λ_{cr} for each profile, in agreement with the values calculated from Eq. (8) and that are shown in Table I.

density profile and no information is necessary about its other physical parameters. The values of λ_{crit} , calculated from Eq. (8) for density profiles that are well-known in the literature, are shown in Table I. For these profiles we also show in Fig. 1 the Einstein angle θ_{*E} as calculated from Eq. (7). As expected, the Einstein angle is the smallest for the WaveDM profile (10) alone, which also means that it is the one with the weakest lensing signal.

We should mention here an additional use of the lens equation (7) to constrain the free parameters of a given density profile. It relates to the fact that any DM halo characterized by a particular density profile needs to satisfy the constraint $\lambda \geq \lambda_{\text{cr}}$ if it is to produce a lensing signal. Using Eqs. (6) and (8), the latter statement can be re-written as

$$\frac{\rho_s r_s}{M_{\odot} \text{pc}^{-2}} \geq 10^3 \frac{h}{0.57} \frac{d_{\text{OS}}}{d_{\text{OL}} d_{\text{LS}}} \lambda_{\text{cr}}. \quad (9)$$

Equation (9) establishes a minimum value for the (structural) surface density $\rho_s r_s$ of any given DM profile in

¹ This is the same parameter used in Ref. [35], but also see Ref. [39] in which the definition of λ differs by just a factor of $1/4\pi$.

² It should be noted that the definition of λ_{cr} depends on the chosen scale radius for normalization r_s , so that the value obtained from Eq. (8) in our case is considering that r_s is coincides with the intrinsic distance scale in the density profile $\rho(r)$.

terms of the measured quantities of a lens system. Although the constraint Eq. (9) is satisfied automatically by the NFW profile, for which $\lambda_{\text{crit}} = 0$, this is not the case for the other profiles listed in Table I.

B. Combined density profile of WaveDM

For the density profile of WaveDM halos we will consider the model described in Refs. [19, 32], which arises from the study of extensive N-body simulations. The profile consists basically of two parts: one part describing a core sustained by the quantum pressure of the boson particles, also known as the soliton profile, and another part that resembles a NFW-like profile in the outer parts of the halo. As argued in Ref. [41], the transition at some radius to a NFW profile must be expected from the change of behavior to CDM on scales larger than the natural length of coherence, which should be proportional to the associated Compton length of the boson particles.

The soliton profile is

$$\rho_{\text{sol}}(r) = \frac{\rho_s}{(1 + r^2/r_s^2)^8}, \quad (10)$$

where r_{sol} and ρ_{sol} are its characteristic radius and central density contrast, respectively. This profile was first studied in detail in Ref. [32], although here we are following the nomenclature adopted in Ref. [41], where it is also shown that the profile fits well the ground-state solution of the so-called Schrödinger-Poisson (SP) system of equations [33, 34]. In this respect, the soliton profile is strongly related to the wave properties (via the Schrödinger equation) of the boson particles.

One important property of the profile given in Eq. (10) is that it must also obey the intrinsic scaling symmetry of the SP system [34]. If $0 < \hat{\lambda} \ll 1$ is a constant parameter, it can be shown that the central density and radius in the soliton profile are given by

$$\rho_s = \hat{\lambda}^4 m_a^2 m_{\text{Pl}}^2 / 4\pi, \quad r_s = (0.23 \hat{\lambda} m_a)^{-1}, \quad (11)$$

This equation suggests that the intrinsic, physical, quantities of the soliton profile in Eq. (10) are related as defined in Eq. (1), which we rewrite here just for clarity:

$$\frac{\rho_s}{M_{\odot} \text{pc}^{-3}} = 2.4 \times 10^{12} \left(\frac{r_s}{\text{pc}} \right)^{-4} \left(\frac{m_a}{10^{-22} \text{eV}} \right)^{-2}.$$

This relation, Eq. (1) will be important later when we discuss the constraints on the boson mass m_a .

For the NFW profile at the outskirts of the galaxy halo we adopt the following parametrisation

$$\rho_{\text{NFW}}(r) = \frac{\rho_s \rho_{\text{NFW}*}}{\alpha_{\text{NFW}} (r/r_s) (1 + \alpha_{\text{NFW}} r/r_s)^2}. \quad (12)$$

Notice that in writing Eq. (12) we are assuming the following implicit definitions for the scale radius and density, respectively, of the NFW profile: $r_{\text{NFW}} = r_s / \alpha_{\text{NFW}}$

and $\rho_{\text{NFW}} = \rho_{\text{sol}} \rho_{\text{NFW}*}$, where both α_{NFW} and $\rho_{\text{NFW}*}$ are dimensionless numbers.

Unfortunately, there is not precise information in Ref. [19] about the transition in a galaxy halo from the soliton profile of Eq. (10) to the NFW profile of Eq. (12) in the general case. Hence, for the present work we adopt the convention for a combined profile as suggested in Ref. [41]

$$\rho(r) = \Theta(r_{\epsilon} - r) \rho_{\text{sol}}(r) + \Theta(r - r_{\epsilon}) \rho_{\text{NFW}}(r). \quad (13)$$

where $\Theta(r_{\epsilon} - r)$ is the Heavisides step function. Here, r_{ϵ} is the matching radius where the transition between the individual profiles occurs, and which satisfies the condition $\rho(r_{\epsilon}) = \epsilon \rho_s$. Notice that $0 < \epsilon < 1$ if the transition between the profiles is to occur at the outskirts of the galaxy halo.

In general terms, and under our parameterization, there are six free parameters in the combined profile (13): $(\rho_s, r_s, \rho_{\text{NFW}*}, \epsilon, r_{\epsilon}, \alpha_{\text{NFW}})$. We will now derive two new constraints that arise from the continuity of the combined density profile at the matching radius which will help us to reduce the number of free parameters.

For a continuous density function, we must impose the condition

$$\rho_{\text{sol}}(r_{\epsilon}) = \epsilon \rho_s = \rho_{\text{NFW}}(r_{\epsilon}). \quad (14)$$

When Eq. (14) is applied to the soliton profile of Eq. (10), we obtain

$$r_{\epsilon*} = r_{\epsilon}/r_s = \left(\epsilon^{-1/8} - 1 \right)^{1/2}, \quad (15a)$$

which basically establishes the interchangeability of the (dimensionless) matching radius $r_{\epsilon*}$ and ϵ . In the case of the NFW profile (12), the continuity condition (14) establishes that

$$\epsilon^{-1} \rho_{\text{NFW}*} = \alpha_{\text{NFW}} r_{\epsilon*} (1 + \alpha_{\text{NFW}} r_{\epsilon*})^2, \quad (15b)$$

which, taking into account Eq. (15a), can be written as

$$\rho_{\text{NFW}*} = \frac{\alpha_{\text{NFW}} r_{\epsilon*} (1 + \alpha_{\text{NFW}} r_{\epsilon*})^2}{(1 + r_{\epsilon*}^2)^8}. \quad (15c)$$

Equation (15c) indicates the (normalized) density $\rho_{\text{NFW}*}$ that is required for a correct matching between the soliton and NFW profiles, for given values of α_{NFW} and $r_{\epsilon*}$.

However, one can see that the continuity constraint (15c) actually shows a hidden degeneracy: once the values of α_{NFW} and $\rho_{\text{NFW}*}$ are fixed, there can be up to two solutions for the matching radius $r_{\epsilon*}$. This is a direct consequence of the fact that the crossing of the density profiles (10) and (12) can occur at most at two different points, as illustrated in the left-hand panel of Fig. 2, which shows normalized density profiles for $\alpha_{\text{NFW}} = 0.1$ and different values of the normalized density $\rho_{\text{NFW}*}$.

Fig. 2 also shows that there exists a maximum value of $\rho_{\text{NFW}*}$ beyond which the profiles do not cross each other.

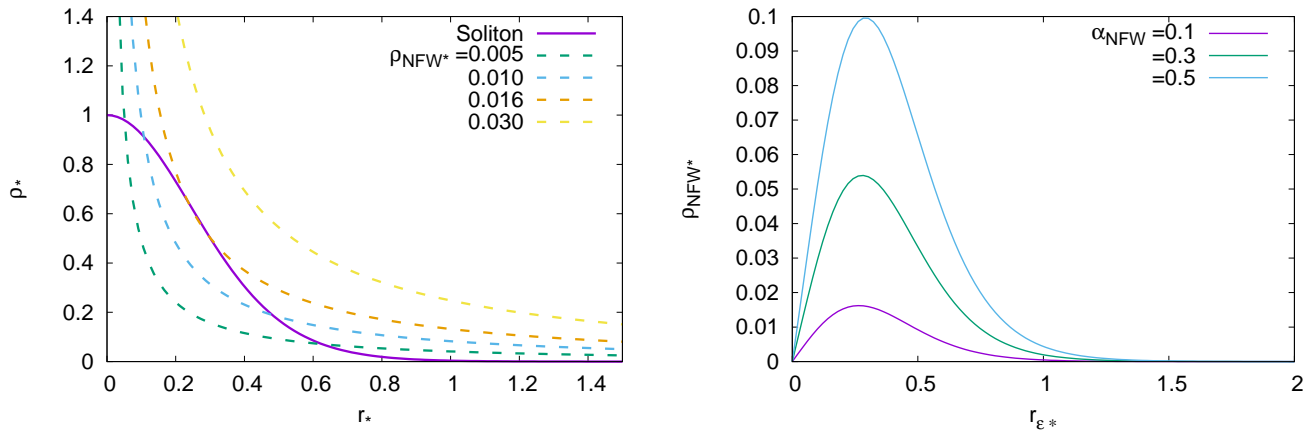


FIG. 2. (Left) The normalized density profile of the soliton, together with different examples of the normalized NFW profile. We show here that there are at most two values of the matching radius r_{ϵ^*} , which depend on the given values of the normalized density ρ_{NFW^*} and α_{NFW} (here we have taken $\alpha_{\text{NFW}} = 0.1$). (Right) The normalized density ρ_{NFW^*} as a function of the matching radius r_{ϵ^*} , for different values of α_{NFW} , as indicated by Eq. (15c). Notice that there are two possible values of r_{ϵ^*} for any given value of ρ_{NFW^*} , except for the maximum value of the latter. This is consistent with the examples shown in the left panel, and the maximum value of ρ_{NFW^*} corresponds to the extreme case in which the soliton profile and NFW profile touch at a single point.

This fact can be understood in terms of Eq. (15c), which we evaluate for different values of α_{NFW} in the right-hand panel of Fig. 2. Here we can see that, for each α_{NFW} , there is always a maximum value of ρ_{NFW^*} that corresponds to the case in which the soliton and NFW density profiles barely touch, in the left-hand panel of Fig. 2.

To avoid the hidden degeneracy, and to select a combined profile with an interior soliton shape, we will choose those cases for which $r_{\epsilon^*} \geq r_{\epsilon^*,\text{max}}$, where $r_{\epsilon^*,\text{max}}$ is the matching radius corresponding to the maximum value of ρ_{NFW^*} . A straightforward calculation from Eq. (15c) shows that $r_{\epsilon^*,\text{max}}$ is a root of the cubic equation

$$13\alpha_{\text{NFW}}r_{\epsilon^*,\text{max}}^3 + 15r_{\epsilon^*,\text{max}}^2 - 3\alpha_{\text{NFW}}r_{\epsilon^*,\text{max}} = 1. \quad (16)$$

Although there is a general solution to this equation, it can be shown that the limits for small and large values of α_{NFW} are

$$\lim_{\alpha_{\text{NFW}} \rightarrow 0} r_{\epsilon^*,\text{max}} = (1/\sqrt{15}), \quad (17a)$$

$$\lim_{\alpha_{\text{NFW}} \rightarrow \infty} r_{\epsilon^*,\text{max}} = (\sqrt{3/13}). \quad (17b)$$

This means that in absolute terms the maximum value of ρ_{NFW^*} must be located in the range $0.25 < r_{\epsilon^*,\text{max}} <$

0.48, which is agreement with the values observed in the right-hand panel of Fig. 2.

In the end, it is possible to reduce the number of free parameters that describe the combined profile (13) to only four: ρ_{sol} , r_{sol} , r_{ϵ} and α_{NFW} . By means of these parameters and the constraints discussed above, the other parameters are fully specified.

One last comment is appropriate. Notice that our chosen normalization is such that the physical parameters in the NFW profile (12) are given in terms of those in the soliton profile (10). This means, for instance, that $\rho_{\text{NFW}^*} > 1$ ($\rho_{\text{NFW}^*} < 1$) is equivalent to $\rho_{\text{NFW}} > \rho_s$ ($\rho_{\text{NFW}} < \rho_s$), whatever the physical value of ρ_s is. Likewise, we find that $\alpha_{\text{NFW}} < 1$ ($\alpha_{\text{NFW}} > 1$) corresponds to $r_{\text{NFW}} > r_s$ ($r_{\text{NFW}} < r_s$), even if the physical value of r_s is not known beforehand. The same will apply for the matching radius, since $r_{\epsilon^*} > 1$ ($r_{\epsilon^*} < 1$) means that matching occurs beyond the soliton radius and then $r_{\epsilon} > r_s$ (before the soliton radius, and then $r_{\epsilon} < r_s$).

C. Gravitational Lensing

To obtain the lensing properties of the combined profile given by Eq. (13), we follow the recipe described in Sec. II A. We first need to compute the projected surface mass density (3b). Because of the presence of the step functions in Eq. (13), the integral in Eq. (3b) naturally separates as

$$\Sigma_*(\theta_*, r_{\epsilon*}, \alpha_{\text{NFW}}) = 2 \begin{cases} \int_0^{\sqrt{r_{\epsilon*}^2 - \theta_*^2}} \frac{dz}{(1 + \hat{r}^2)^8} + \frac{r_{\epsilon*} (1 + \alpha_{\text{NFW}} r_{\epsilon*})^2}{(1 + r_{\epsilon*}^2)^8} \int_{\sqrt{r_{\epsilon*}^2 - \theta_*^2}}^{\infty} \frac{dz}{\hat{r} (1 + \alpha_{\text{NFW}} \hat{r})^2}, & \theta_* < r_{\epsilon*}, \\ \frac{r_{\epsilon*} (1 + \alpha_{\text{NFW}} r_{\epsilon*})^2}{(1 + r_{\epsilon*}^2)^8} \int_0^{\infty} \frac{dz}{\hat{r} (1 + \alpha_{\text{NFW}} \hat{r})^2}, & \theta_* \geq r_{\epsilon*}. \end{cases} \quad (18)$$

It should be understood that the integrals in Eq. (18) are done along the line of sight. Notice that in Eq. (18) we are following our convention in Sec. II for normalized quantities, namely $\Sigma_* = \Sigma/(\rho_s r_s)$, $\theta_* = \xi/r_s$ and $z = \sqrt{r_*^2 - \theta_*^2}$. The analytical expression for the integrals in Eq. (18) can be found in appendix A.

Interestingly enough, Eq. (18) shows that the projected surface mass density only depends upon the characteristic radii of the combined density profile (13). Actually, it is the (normalized) matching radius $r_{\epsilon*}$ which determines the general behaviour of Σ_* . For instance, it can

be shown that

$$\lim_{r_{\epsilon*} \rightarrow \infty} \Sigma_*(\theta_*, r_{\epsilon*}, \alpha_{\text{NFW}}) = 0.658 (1 + \theta_*^2)^{-15/2}, \quad (19)$$

a result that is obtained from the first branch in Eq. (18). Notice that Eq. (19) is exactly the result for the soliton profile (10) alone. Also, we cannot recover the result of the NFW profile if $r_{\epsilon*} \rightarrow 0$, as the second branch in Eq. (19) indicates that $\Sigma_* \rightarrow 0$ in such a case. In addition, it must be remembered that the operation $r_{\epsilon*} \rightarrow 0$ is not permitted by the constraint $r_{\epsilon*} \geq r_{\epsilon*, \text{max}}$, see Eq. (16).

Going back to the complete profile (13), we start with the calculation of the critical value λ_{crit} from the analytical formula (8). The (total) projected surface mass density for the special value $\theta_* = 0$ is obtained from the first branch of the solution (18) as

$$\Sigma_*(0, r_{\epsilon*}, \alpha_{\text{NFW}}) = 2 \left[\int_0^{r_{\epsilon*}} \frac{dz}{(1 + z^2)^8} + \frac{r_{\epsilon*} (1 + \alpha_{\text{NFW}} r_{\epsilon*})^2}{(1 + r_{\epsilon*}^2)^8} \int_{r_{\epsilon*}}^{\infty} \frac{dz}{z (1 + \alpha_{\text{NFW}} z)^2} \right], \quad (20)$$

which indicates, together with Eq. (7), that the critical value λ_{cr} of the combined profile (13) is a function of $r_{\epsilon*}$ and α_{NFW} , and its behavior for different combinations of these parameters is shown in the left panel of Fig. 3. Not surprisingly, the addition of the NFW outer part helps the soliton profile to achieve small values of λ_{crit} , which in turn eases the accomplishment of the inequality (9).

In particular, Fig. 3 shows that $\lambda_{\text{crit}} \rightarrow 0$ as $\alpha_{\text{NFW}} \rightarrow 0$, which means that the combined profile (13) will be able to produce a lensing signal for any non-trivial combination of its parameters ρ_s and r_s .

In the case of the combined profile (13) the total mass M inside a sphere of any given radius $r > r_{\epsilon}$ is simply given by the integral

$$\frac{M(r)}{10^{13} M_{\odot}} = 3 \left(\frac{m_a}{10^{-22} \text{ eV}} \right)^{-2} \left(\frac{r_s}{\text{pc}} \right)^{-1} \times \left[\int_0^{r_{\epsilon*}} \frac{dx x^2}{(1 + x^2)^8} + \frac{r_{\epsilon*} (1 + \alpha_{\text{NFW}} r_{\epsilon*})^2}{(1 + r_{\epsilon*}^2)^8} \int_{r_{\epsilon*}}^{r_*} \frac{dx x}{(1 + \alpha_{\text{NFW}} x)^2} \right]. \quad (21)$$

In the general case the total mass diverges as $r \rightarrow \infty$, whereas for the soliton profile only (which requires $r_{\epsilon*} \rightarrow \infty$) we simply obtain that its total mass M_s is [31, 34, 41]

$$\frac{M_s}{10^{11} M_{\odot}} = 7.7 \left(\frac{m_a}{10^{-22} \text{ eV}} \right)^{-2} \left(\frac{r_s}{\text{pc}} \right)^{-1}. \quad (22)$$

In general, we expect from Eq. (21) the total mass in

the combined profile to be larger than the soliton alone, that is $M(r) \geq M_s$. However, the value of the total mass M will depend on the upper limit of integration r_* , and the largest values for any given r_* will be obtained for the case where $\alpha_{\text{NFW}} \rightarrow 0$, similar to the case of the critical value λ_{crit} . The aforementioned general behaviour of the total mass M as a function of the free parameters $r_{\epsilon*}$ and

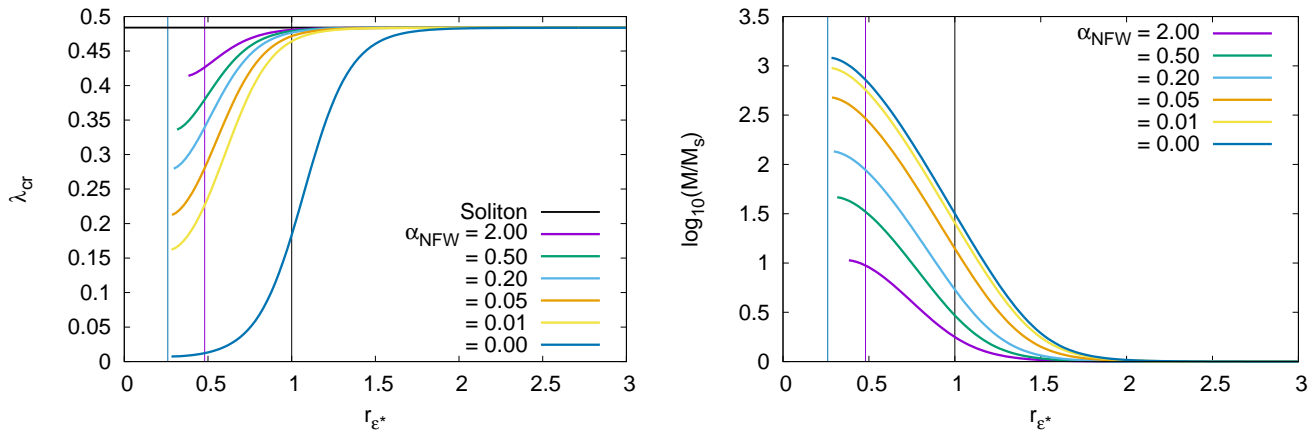


FIG. 3. (Left) The critical value λ_{cr} as a function of r_{ϵ^*} for different values of α_{NFW} , see Eqs. (8) and (20). Notice that the critical value corresponding to the soliton case, $\lambda_{\text{cr}} \simeq 0.48$, is obtained asymptotically in the limit $r_{\epsilon^*} \rightarrow \infty$. Notice that in plotting the curves we have taken into account the constraint $r_{\epsilon^*} \geq r_{\epsilon^*,\text{max}}$, see Eq. (16). Moreover, it can be seen that the lowest value of λ_{cr} , for any given value of α_{NFW} , is indeed attained at $r_{\epsilon^*,\text{max}}$. (Right) The same as before but now for the total mass M in Eq. (21), with its value normalized in terms of the soliton mass M_s given in Eq. (22). Notice that the latter is the asymptotic value at large r_{ϵ^*} , whereas for small values of the latter the total mass M can be three orders of magnitude larger than the soliton mass M_s . Here the upper limit of integration in Eq. (21) was taken as $r_* = 20$. The vertical black line in both plots marks the position of the soliton radius, in dimensionless units, at $r_{\epsilon^*} = 1$. Also, the values of the soliton profile alone correspond to the limit $\alpha_{\text{NFW}} \rightarrow \infty$. See the text for more details.

α_{NFW} is shown in the right-hand panel of Fig. 3. For the numerical examples we considered the upper limit of integration $r_* = 20$, for which we then see that the difference between M and M_s can be as large as three orders of magnitude in the case $\alpha_{\text{NFW}} = 0$.

III. DATA ANALYSIS

In this section we will use our theoretical results to infer information about the WaveDM profile from observations of specific lens systems. For this we will use data from the SLAC survey [42]. To do so, we recall from Sec. II B that there are four free parameters that are needed to describe the lensing properties of the combined density profile, Eq. (13). However, the lens equation, (4), discussed in Sec. II C, is not explicitly dependent of two of them, namely ρ_s and r_s , but only to the free parameters of the NFW outer profile r_{ϵ^*} and α_{NFW} . Therefore we could use the right-hand side of the lens equation (4) to put constraints on the surface density through the combination of parameters $\rho_s r_s$ – see the discussion in Sec. II A.

However, the special properties of the WaveDM profile, as represented by Eq. (1), suggest that the lens equation could be written in a more convenient form. Using that the (normalized) angular Einstein radius is $\theta_{*E} = R_E/r_s$, Eq. (6) can be re-cast in the form

$$m_{a22}^{-2} \theta_{*E} m_*(\theta_{*E}, \alpha_{\text{NFW}}, r_{\epsilon^*}) = \frac{1}{2.4} \frac{d_{\text{OS}}}{d_{\text{OL}} d_{\text{LS}}} \frac{h}{0.57} \left(\frac{R_E}{\text{kpc}} \right)^3, \quad (23)$$

where we have set $m_{a22} \equiv m_a/10^{-22}\text{eV}$. Equation (23) then defines a different observable, which results solely from the combination of the distances involved in the measurement of the lens system, so that we can put constraints directly on the boson mass m_a rather than on the energy density ρ_s , but in any case in combination with the rest of parameters, namely θ_{*E} , α_{NFW} , and r_{ϵ^*} .

Name	$f_{*,\text{Ein}}^{\text{Salp}}$	z_{lens}	z_{source}	$d_{\text{OS}}/(d_{\text{OL}}d_{\text{LS}})$	R_E
J0008-0004	0.50 ± 0.16	0.44	1.192	6.609565	6.59
J0935-0003	0.35 ± 0.05	0.347	0.467	18.04391	4.26
J0946+1006	0.46 ± 0.13	0.222	0.609	9.700301	4.95
J1143-0144	0.46 ± 0.10	0.106	0.402	14.9161	3.27
J1306+0600	0.47 ± 0.08	0.173	0.472	11.66306	3.87
J1318-0313	0.42 ± 0.08	0.24	1.3	7.215974	6.01

TABLE II. List of selected galaxies from SLACS. These were selected because they have a fraction of luminous matter of 0.5 or less; see the values in the second column. Column (1) gives the label of the galaxies within the SDSS catalog, column (2) indicates the type of the galaxy. Column (6) lists the measured Einstein radius in units of kpc.

In general, we expect that, given the data from a single galaxy, there will always be a region in the parameter space that will satisfy Eq. (23). Thus, for a given sample

of galaxies, we could in principle determine the range of possible values of m_a that is consistent with the observed data. However, we must recall that the boson mass m_a is a fundamental physical parameter of the model which in principle should have a unique value. This means that the boson mass should be treated differently from other parameters in the model and should *not* be given the freedom to vary from galaxy to galaxy.

Our proposal, therefore, is to study the lensing properties of the WaveDM profile by fixing the value of the boson mass and finding, via statistical analysis, the best-fit values of the remaining free parameters θ_{*E} , α_{NFW} and $r_{\epsilon*}$. As we are interested in the properties of the WaveDM profile alone, we will select a sample of galaxies from the SLAC catalog for which the DM component is the dominant contribution – that is, with a fraction of luminous matter of 50% or less. The selected galaxies are shown in Table II, together with the values of their lens parameters.

A. Soliton core profile

As a first case of study, let us consider the soliton core profile without the external NFW part. There are in this case only two free parameters: m_{a22} and θ_{*E} . The projected mass surface density given by Eq. (5a), with the help of Eq. (19), has in this case an analytical expression,

$$m_*(\theta_{*E}) = \frac{2}{13\lambda_{\text{crit}}} \frac{(1 + \theta_{*E}^2)^{13/2} - 1}{(1 + \theta_{*E}^2)^{13/2}}, \quad (24)$$

where $\lambda_{\text{crit}} \simeq 0.484$ is the critical value calculated from Eq. (8); see also Table I. Notice that $m_*(0) = 0$, whereas its asymptotic limit is $m_*(\infty) = 2/(13\lambda_{\text{crit}})$.

To obtain a basic understanding of the solutions that will be found for the physical parameters, we show in the top panel of Fig. 4 the expected behavior of the left-hand side of Eq. (23) as a function of the Einstein angle θ_{*E} . We also show, as the series of horizontal lines, the values of the right-hand side of Eq. (23) obtained from the observed data for the galaxies listed in Table II.

Figure 4 shows that it will always be possible to identify a value of the Einstein angle θ_{*E} for which the left-hand and right-hand sides of Eq. (23) are in agreement, irrespective of the value of the boson mass – although as the boson mass increases the agreement occurs at increasingly large values of θ_{*E} . For the examples shown in Fig. 4, a boson mass of order $m_{a22} \simeq 0.02$ seems to fit well the SLACS galaxies listed in Table II – corresponding to an allowed range for the angular Einstein radius of $5 < \theta_{*E} < 10$. This latter range can also be translated into an allowed range for the soliton radius, and suggests that $r_{\text{sol}} \sim \text{kpc}$ for the given example galaxies.

To summarise, given that we have only one observable constraint, the most we can do is first to fix the value of the boson mass m_a and from this to obtain constraints on the remaining free parameters that are consistent with

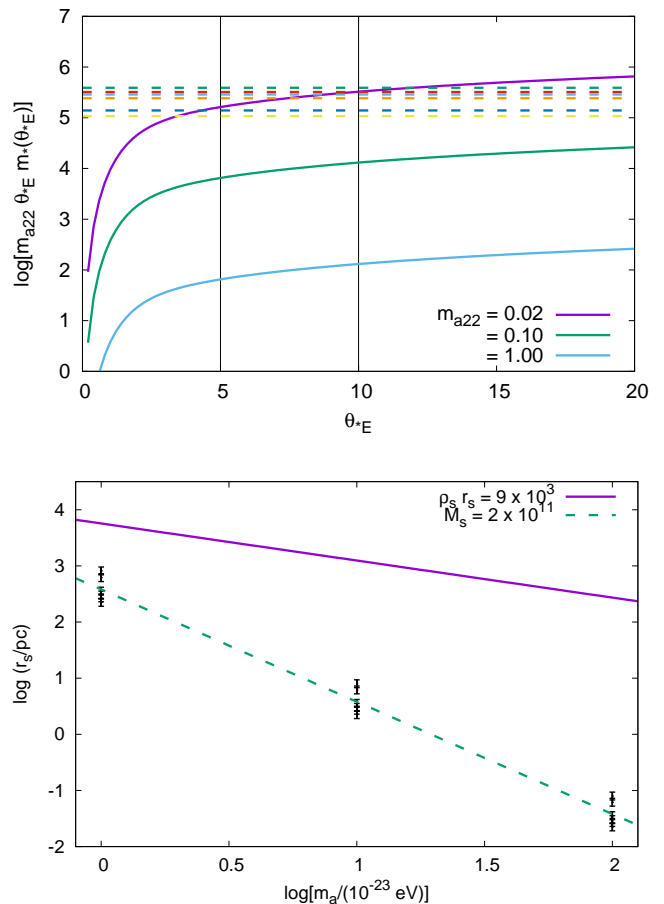


FIG. 4. (Top) Illustration of how we can use Eq. (23) to constrain the parameters of the WaveDM model. The curves show, for selected values of the boson mass m_{a22} , how the left-hand side of Eq. (23) varies as a function of the Einstein angle θ_{*E} . The dashed horizontal lines represent, for each galaxy in our sample, the corresponding value inferred from observations – i.e. using the right-hand side of the aforementioned equation. From these examples, it can be seen that the preferred values of the boson mass appear to be $m_{a22} \simeq 0.02$. However, note that it is always possible to find a solution that matches the left-hand and right-hand sides of Eq. (23), for any given value of the boson mass m_a , by suitably large choice of Einstein angle θ_{*E} . (Bottom) The best fit values of the soliton radius r_s shown in Table III for fixed values of the boson mass m_a . Because the main constraint imposed by the lensing system is for the total mass inside the Einstein radius R_E , the obtained data points lie along the line of constant soliton mass $M_s \simeq 2 \times 10^{11} M_\odot$. The data points also lie below the line representing the inequality (9) for the surface density $\rho_s r_s = 9 \times 10^3 M_\odot \text{pc}^{-2}$. See the text for more details.

that boson mass. Specifically, by adopting a proposed value for the boson mass m_a in Eqs. (23) and (24), we can obtain for each galaxy the corresponding best-fit value for θ_{*E} , and from that the best-fit value for r_s .

The results obtained for our selected sample of galaxies are shown in Table III, and also plotted in the bottom

panel of Fig. 4. The latter figure speaks for itself, and it shows that the data points for all galaxies lie along the line with a constant soliton mass $M_s \simeq 10^{11} M_\odot$ (see Eq. (22)), and (as required) all lie below the line that represents the inequality (9) for the galaxy in Table II (J0935-0003) with the most extreme value for the ratio of distances on the right-hand side of Eq. (23). The different values obtained for the characteristic radius r_s give an enclosed mass which corresponds closely to the values reported in [42]. Nevertheless, these models are found to be considerably too compact when the characteristic radius and corresponding enclosed mass are considered together. For example, galaxy J0008-0004 has a value for $M_{Eins} = 3.1 \times 10^{11} M_\odot$ which is comparable with the value of $M_s = 3.4 \times 10^{11} M_\odot$ obtained using the best fit parameters of the soliton model. Notwithstanding that the soliton model gives an enclosed mass that is adequate and realistic, we think that the characteristic radius is most definitely not so. The mean effective radius for this galaxy is observed to be $r_e \approx 9.6$ kpc, which is several orders of magnitude larger than the characteristic radius r_s obtained for any of the different boson masses presented in Table III. Therefore we think the soliton profile alone is actually not helping to explain the distribution of dark matter around the selected galaxies in a consistent way.

	$m_{a22} = 10$	$m_{a22} = 1$	$m_{a22} = 0.1$
Galaxy	$\log_{10}(r_s/\text{pc})$		
J0008-0004	$-1.65^{+0.07}_{-0.06}$	$0.35^{+0.07}_{-0.06}$	$2.35^{+0.07}_{-0.06}$
J0935-0003	$-1.52^{+0.07}_{-0.06}$	$0.48^{+0.07}_{-0.06}$	$2.48^{+0.07}_{-0.06}$
J0946+1006	$-1.45^{+0.07}_{-0.06}$	$0.55^{+0.07}_{-0.06}$	$2.55^{+0.07}_{-0.06}$
J1143-0144	$-1.10^{+0.07}_{-0.06}$	$0.90^{+0.07}_{-0.06}$	$2.91^{+0.07}_{-0.06}$
J1306+0600	$-1.21^{+0.07}_{-0.06}$	$0.79^{+0.07}_{-0.06}$	$2.79^{+0.07}_{-0.06}$
J1318-0313	$-1.57^{+0.07}_{-0.06}$	$0.43^{+0.07}_{-0.06}$	$2.43^{+0.07}_{-0.06}$

TABLE III. The values of the soliton radius in the logarithmic scale $\log_{10}(r_s/\text{pc})$ obtained from the fits to the indicated galaxies, for three different values of the boson mass m_a . The data points are also shown in the bottom panel of Fig. 4, where we see that they all indicate that the total mass contained within the Einstein radius is $M_s \simeq 10^{11} M_\odot$.

There are two valuable lessons from the above exercise. The first one is that the soliton core profile alone will always be able to fulfill the lensing constraints even without the consideration of the NFW contribution. This is not surprising, as the lensing equations can be solved even if we consider a point particle with the required total mass (which formally corresponds to the soliton core profile with $m_a \rightarrow \infty$). The second lesson is that even though the soliton profile may be adequate, formally speaking, to explain the lensing properties of the galaxies in Table II,

we will, in any case, have to consider the NFW outskirts in the complete profile (13) in order to satisfy other constraints that suggest that the boson mass should be in the range $m_{a22} = 1 - 10$ [43].

B. Complete profile

Taking into account the above experience gained with the soliton profile alone, we will now consider the following procedure for the complete WaveDM profile.

Since the total mass inside the Einstein radius is the only constraint provided by the lens systems, we will fix the values of the boson mass m_a and soliton mass M_s . For this, we take following values of the boson mass $m_{a22} = 0.1, 1, 10$, and for the soliton mass $\log_{10}(M_s/M_\odot) = 11.5, 10.5, 9.5, 8.5, 7.5$, from which we will calculate the values of r_s by means of Eq. (22).

We will adopt a uniform prior for the other parameters over the following ranges: $\alpha_{\text{NFW}} = [0 : 10]$, and $r_{\epsilon*} = [r_{\epsilon*,\text{max}} : 10]$. Here $r_{\epsilon*,\text{max}}$ is found from the cubic equation (16) for a given value of α_{NFW} , and the extreme values $\alpha_{\text{NFW}} = 10$ and $r_{\epsilon*} = 10$ are suggested by Figs. 3 and 4.

We will obtain the values of θ_{*E} by sampling from a Gaussian distribution, using the relation

$$\theta_{*E}(p) = \theta_{*Em} + \sigma\sqrt{2}\text{erf}^{-1}(2p - 1), \quad p \in (0, 1). \quad (25)$$

The value for $\theta_{*Em} = R_E/r_s$ is the mean of the distribution using the observed value for the Einstein radius, and $\sigma = 0.05 * \chi$ the error assigned. p is a random number sampled from a uniform distribution on the interval $[0, 1]$. The inverse error function is approximated as described in [44]. In this way, the variable θ_{*E} will not otherwise enter into the fitting analysis.

Once the soliton mass is fixed, the rest of the mass that is included within the Einstein radius must be completed by the NFW profile. Because this requires a huge contribution, up to three orders of magnitude more, one sensible consideration is to include a simple approximation of a partial contribution of the luminous matter inside the Einstein radius. In a first approximation, the mass corresponding to the barionic matter is simply a constant value modeled as a point particle. This is done from Eq. (2), and then the projected mass for the lens is composed of two parts,

$$m'(\theta) = m(\theta) + M', \quad (26)$$

where $m(\theta)$ is the mass from the dark matter component given by the profile in Eq. (13), and $M' = f_{*,Eins} M_{Eins}$ is the stellar mass contribution as described in Table II. These values are normalized accordingly and then the dimensionless total mass m' is

$$m'_*(\theta_{*E}, \alpha_{\text{NFW}}, r_{\epsilon*}) = m_*(\theta_{*E}, \alpha_{\text{NFW}}, r_{\epsilon*}) + M'_*, \quad (27a)$$

where

$$M'_* = 0.3208 f_{*,Ein} \left(\frac{M_{Ein}}{M_s} \right). \quad (27b)$$

Eq. (27a) is combined with Eq. (23) to produce a modified observable which uses the soliton mass directly,

$$\frac{M_s}{M_\odot} m'_*(\theta_{*E}, \alpha_{NFW}, r_{\epsilon*}) = \frac{7.7 \times 10^8}{2.4} \frac{d_{OS}}{d_{OL} d_{LS}} \frac{h}{0.57} \left(\frac{R_E}{\text{kpc}} \right)^2 \quad (28)$$

C. General results

Using the Sloan Lens ACS Survey (SLACS) data for several lens candidates with strong lensing [37, 42], we will try to constrain the free parameters that will satisfy Eq. (28). As said before, the information available from the data is the Einstein radius, R_E , the lens distances (d_{OL} , d_{LS} , d_{OS}), and the redshift, z , of the lens. This information is used in the Multinest code [45] to carry out a parameter search for each individual galaxy.

Typical results are shown in Fig. 5 for the individual cases of galaxies J0008-0003 and J0008-0004; both cases include the contribution of the luminous matter to the total mass of the lens as in Eq. (28). For the purposes of clarity, in each figure we indicate the radius r_s and total mass M_s of the soliton profile. Some general features of the results are as follows. First, we note that the free parameters $r_{\epsilon*}$ and α_{NFW} appear well constrained if the soliton mass cannot provide the total mass required by the lens system; in the examples shown, this happens if $M_s < 10^{11.5} M_\odot$. The credible regions for the parameters in Fig. 5 are in agreement with the theoretical expectations discussed in Sec. II B: that there is a minimum value for $r_{\epsilon*}$ due to the constraint imposed by Eq. (16), and a maximum value of α_{NFW} appears due to the maximal contribution of the NFW part of the profile to the total mass in the lens, see also the right panel in Fig. 3. Likewise, notice that as $\alpha_{NFW} \rightarrow 0$ the value of the matching radius $r_{\epsilon*}$ is very well constrained, and this is easily understood from Eq. (21): it is $r_{\epsilon*}$ which determines alone the contribution of the NFW part of the profile to the total mass. Finally, observe that the value $\log_{10}(M_s/M_\odot) = 7.5$ is excluded because the code is not able to find any suitable values of the variables that could fit the data. That is, the soliton mass M_s is so small that the NFW part cannot compensate the required mass for the lens.

In summary, if the soliton is allowed to provide enough mass to fulfill the matter contribution in the lens, say $M_s \sim 10^{11.5} M_\odot$, the analysis will select large values for $r_{\epsilon*}$ so that the NFW tail contribution to the total matter is minimal, see Eq. (21). In contrast, if the soliton mass is not large enough, $M_s < 10^{11.5} M_\odot$, it is then possible to find appropriate pairs $(\alpha_{NFW}, r_{\epsilon*})$ for the NFW part of the profile to provide the needed mass for the lens. In this respect, the stripped credible regions in Fig. 5

represent the degeneracy regions in the plane $(\alpha_{NFW}, r_{\epsilon*})$ for the same mass contribution of the NFW tail to the lens system.

Another quantity of interest is the resultant density profile of DM in the lens system. Fig. 6 shows examples of the density profiles inferred from the posteriors of galaxy J0008-0004 in Fig. 5 for a boson mass $m_{a22} = 1$. The soliton core is clearly seen in all curves, and so too is the transition to the NFW part of the profile. Not surprisingly, the largest core corresponds to the configuration with the lowest soliton mass for which the matching radius is close to the lower bound suggested in Eq. (17a).

We also report in Fig. 7 the results obtained for the lens system J0008-0004, for larger or smaller values of the boson mass. For a mass of $m_{a22} = 10$, the soliton is much more compact, and it is not by itself adequate to describe a galaxy. But given the fact that the parameters α_{NFW} and $r_{\epsilon*}$ are also well constrained we conclude that the lensing effect must be mostly attributed to the NFW part. This is not surprising, as we had already indicated in Sec. II C that strong lensing could be achieved if $\alpha_{NFW} \ll 1$. Moreover, a larger boson mass is also in better agreement with recent cosmological constraints [27] and with estimations based upon satellite galaxies of the Milky Way and Andromeda [46].

In contrast, we can see that the constraints become more diffuse if we consider a smaller boson mass of $m_{a22} = 0.1$, although there seems to be some preference for the case in which $M_s = 10^{10.5}$, that also corresponds to a larger soliton radius. This time the resultant configuration would be in agreement with those found in the statistical analysis made in Ref. [30], which suggests that satellite galaxies put an upper bound on the boson mass that takes the form $m_{a22} < 0.4$.

IV. CONCLUSIONS

We have studied the properties of the so-called WaveDM density profile assuming that it comprises the total DM contribution in galaxies for which a gravitational lens has been detected and measured. In doing so we have adapted the standard lens equations to the particular features of the WaveDM, in that we took into account its soliton core together with its NFW envelope, which is the complete form suggested by numerical simulations of cosmological structure under the WaveDM hypothesis.

We then used the lens equations to make a comparison with actual observations of some lens systems that seem to be DM dominated, although we took into account their baryonic components in a simplified manner. In doing the statistical analysis we considered carefully the role of the different free parameters of the WaveDM profile, in particular the boson mass m_a which has to be regarded as a fundamental parameter that should not vary from one galaxy to another.

The overall procedure was then to fix the value of the

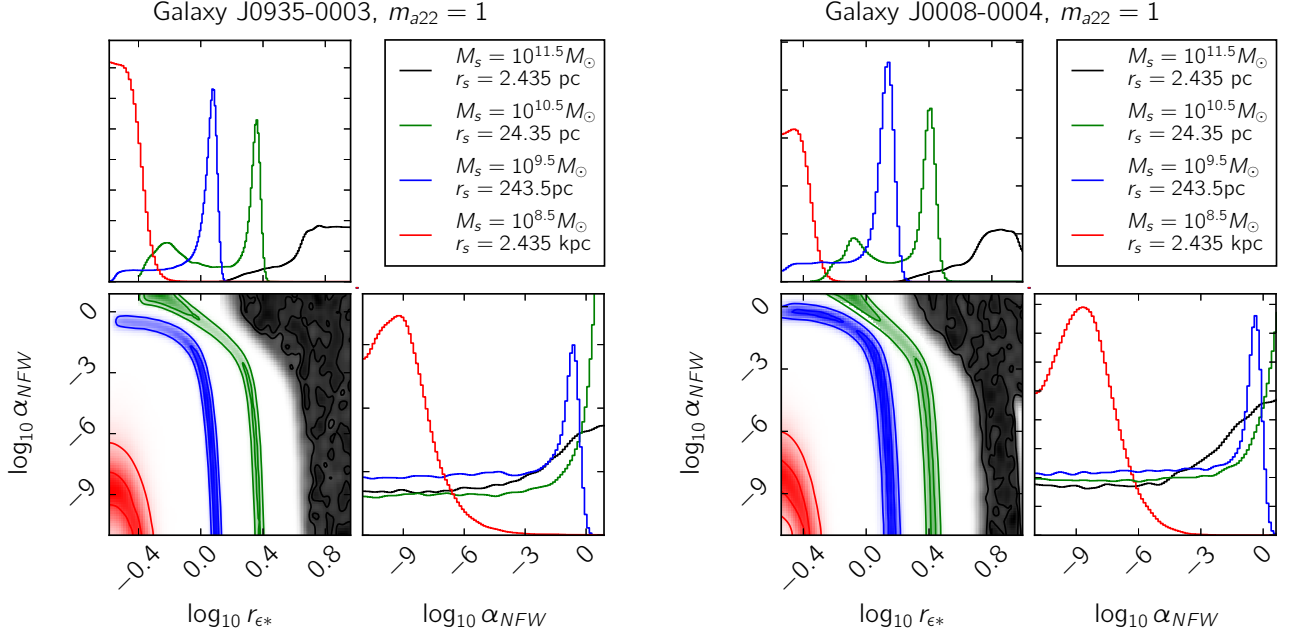


FIG. 5. Triangle plot for the parameter posteriors fitted to galaxies J0008-0003 (left) and J0008-0004 (right). The contribution of the luminous matter is 35% (50%) of the total reduced mass inside the Einstein radius for J0008-0003 (J0008-0004), see also Eq. (28). The colors indicate different choices for the soliton mass M_s , and the values of the corresponding r_s , calculated from a fixed (normalized) boson mass $m_{a22} = 1$, are also shown for comparison. In general, we can see that distinct credible regions can be found for the NFW parameters if the soliton mass is $10^{8.5} < M_s/M_\odot < 10^{11.5}$, and that the constraints are in agreement with the semi-analytic analysis in Sec. II.

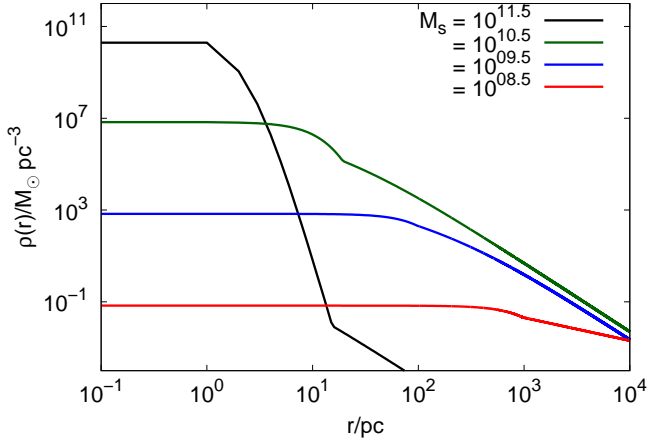


FIG. 6. Comparative plot of the density profiles from selected configurations for Galaxy J0008-0004 obtained from the constraints in Fig. 5. We can clearly see a core region in the center, and that the transition to a NFW-like profile happens at larger radii if the central density is smaller. To draw the plots we chose the value $\alpha_{NFW} = 1$, except in the case $M_s = 10^{8.5} M_\odot$ (red line) for which $\log(\alpha_{NFW}) = -7$. The corresponding matching radius r_e , in full units, is selected to be at 15.36 pc, 19.34 pc, 96.94 pc and 969.4 pc for the soliton masses $10^{11.5} M_\odot$, $10^{10.5} M_\odot$, $10^{9.5} M_\odot$ and $10^{8.5} M_\odot$, respectively.

boson mass and the total mass within the soliton core in the configuration. In consequence, the soliton radius was fixed and the only free parameters were those of the NFW part of the density profile. In general terms, for large or small values of the boson mass, our results indicate that the soliton structure, if it is as massive as $10^{11.5} M_\odot$, is able to fit the measured Einstein radius in the lens systems, although this also requires the soliton structure to be extremely small when compared to the measured scales of the lensing galaxies. This result then indicates that galaxies in general cannot be explained by the soliton structure alone.

Because of the above, we had to consider the complete WaveDM density profile and constrain the NFW free parameters. Generically, and so far for the cases we explored, our analyses suggest that the matching radius for the soliton and NFW parts of the profile is of the same order of magnitude as the soliton radius, $r_e \sim r_s$, which is in agreement with the expectation from numerical simulations[47–49]. In addition, the second free parameter is in general bounded from above as $\alpha_{NFW} < 1$, which just means that the characteristic NFW radius is larger than the soliton radius, $r_{NFW} > r_s$. Moreover, our results also suggest that the case $\alpha_{NFW} \rightarrow 0$ is also possible, which in turn means that the density profile decays as $\rho \sim r^{-1}$ at large radii.

On the other hand, for any given value of the boson mass, it was not possible to constrain the NFW param-

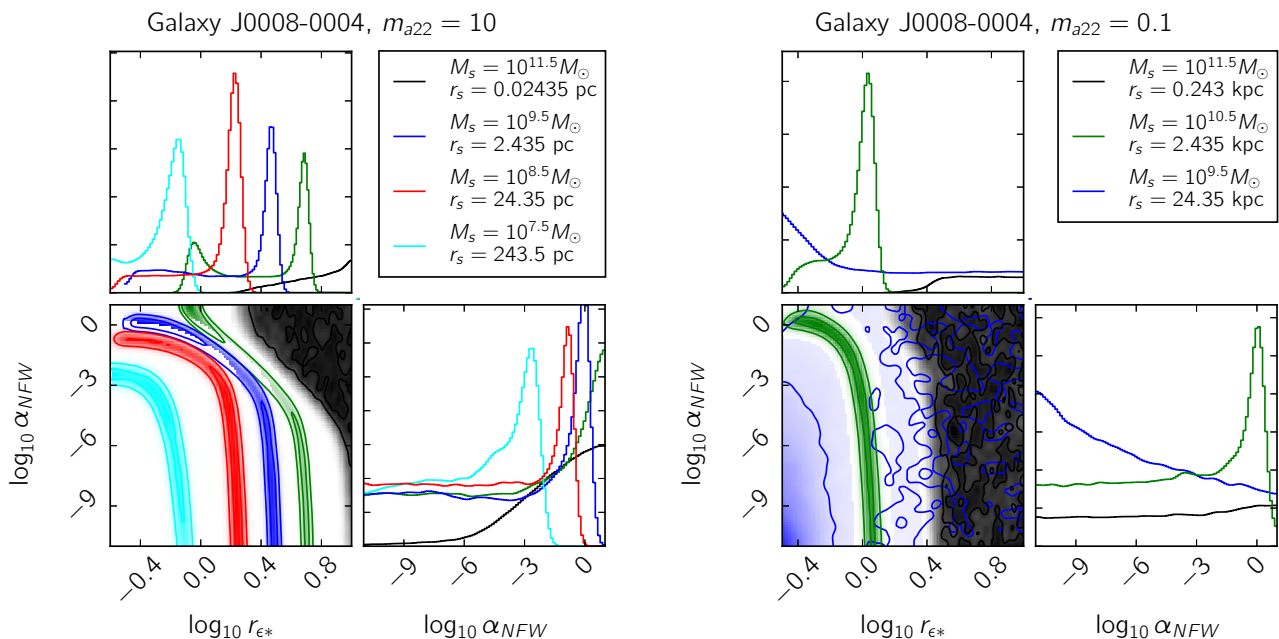


FIG. 7. Triangle plot for the posteriors of galaxy J0008-0004 considering different boson masses m_a . (Left) For the boson mass $m_{a22} = 10$ we obtain good constraints on the NFW parameters, but the soliton core is very compact in all cases. For the case of $M_s = 10^{6.5} M_\odot$ a constraint cannot be found. The line colours represent the same masses as Figure .5. (Right) For the boson mass of $m_{a22} = 0.1$, we can only obtain well defined constraints on the NFW parameters when the soliton mass is $M_s = 10^{10.5} M_\odot$, but not for larger or smaller values. Low values of M_s imply values of the soliton radius r_s that are larger than the Einstein radius, and this kind of cases are unable to satisfy the lensing constraints.

eters in the case where the soliton radius was larger than the Einstein radius, as in such cases the soliton mass is insufficient to produce the required lensing signal. Together with the aforementioned difficulty that the soliton should not provide the whole mass of the lens, we can summarize our results as $M_s/M_\odot < 10^{11.5}$ and $r_s < 6$ kpc. By means of Eq. (22), the above inequalities can be combined in the following lower bound on the boson mass $m_a > 10^{-24}$ eV. Notice that this lower bound is in agreement with previous constraints from cosmological and galactic scales, see for instance[22, 30, 31, 46]. Although the lens systems we considered are not able to put strong bounds on the boson mass, they certainly indicate that most likely a complete WaveDM profile (i.e. comprising a soliton core + NFW tail) is necessary to account for all the diverse observations at galaxy scales.

As a final note, the lens systems studied here have a subdominant, although non-negligible, baryonic contribution. We expect to extend our analysis to a larger sample with a more detailed, specific, inclusion of the baryonic matter that could give us better constraints on the soliton features. This is ongoing work that will be

presented elsewhere.

ACKNOWLEDGMENTS

AH-M acknowledges CONACyT for financial support. LAU-L wishes to thank Andrew Liddle and the Royal Observatory, Edinburgh, for their kind hospitality in a fruitful sabbatical stay. This work was partially supported by Programa para el Desarrollo Profesional Docente; Dirección de Apoyo a la Investigación y al Posgrado, Universidad de Guanajuato, research Grant No. 732/2017 and 878/2017; Programa Integral de Fortalecimiento Institucional; CONACyT México under Grants No. 232893 (sabbatical), No. 167335, No. 179881, No. 269652, No.182445, No. 359103 and Fronteras 281; Fundación Marcos Moshinsky; and the Instituto Avanzado de Cosmología Collaboration.

Appendix A: Integral solutions

Some useful analytical solutions are given here for the integrals in Eq. (18). For the first branch $\theta_* < r_{\epsilon*}$ the formula for the first integral is

$$\int_0^{\sqrt{r_{\epsilon_*}^2 - \xi_*^2}} \frac{dz}{[1 + \alpha_{\text{sol}}^2 \hat{r}^2]^8} = \frac{\alpha_{\text{sol}}^{-1}}{(1 + \alpha_{\text{sol}}^2 \xi_*^2)^{15/2}} \int_0^x \cos^{14} u \, du, \quad \tan x = \alpha_{\text{sol}} \left(\frac{r_{\epsilon_*}^2 - \xi_*^2}{1 + \alpha_{\text{sol}}^2 \xi_*^2} \right)^{1/2}, \quad (\text{A1})$$

where

$$\int_0^x \cos^{14} u \, du = \frac{429}{2048} x + \frac{1001}{16384} \left[3 \sin(2x) + \sin(4x) + \frac{1}{3} \sin(6x) + \frac{1}{11} \sin(8x) + \frac{1}{55} \sin(10x) + \frac{1}{429} \sin(12x) + \frac{1}{7007} \sin(14x) \right], \quad (\text{A2})$$

whereas for the second integral we obtain

$$\int_{\sqrt{r_{\epsilon_*}^2 - \xi_*^2}}^{\infty} \frac{dz}{\hat{r} (1 + \alpha_{\text{NFW}} \hat{r})^2} = \begin{cases} \frac{1}{x^2 - 1} \left(1 - \frac{\sqrt{y^2 - x^2}}{1 + y} - \frac{2 \operatorname{arctanh} \left[\frac{\sqrt{1 - x^2}}{1 + y + \sqrt{y^2 - x^2}} \right]}{\sqrt{1 - x^2}} \right) & x < 1, \\ \frac{1}{3} \left(1 - \frac{y + 2}{y + 1} \sqrt{\frac{y - 1}{y + 1}} \right) & x = 1, \\ \frac{1}{x^2 - 1} \left(1 - \frac{\sqrt{y^2 - x^2}}{1 + y} - \frac{2 \operatorname{arctan} \left[\frac{\sqrt{x^2 - 1}}{1 + y + \sqrt{y^2 - x^2}} \right]}{\sqrt{x^2 - 1}} \right) & x > 1. \end{cases} \quad (\text{A3})$$

where $x = \alpha_{\text{NFW}} \xi_*$ and $y = \alpha_{\text{NFW}} r_{\epsilon_*}$. By setting $y = x$, which is equivalent to $r_{\epsilon_*} = \xi_*$, in Eq. (A3) we obtain the solution for the second branch in Eq. (18). For the case $\xi_* = 0$, which is used in Eq. (20), the integral result simply is

$$\int_{r_{\epsilon_*}}^{\infty} \frac{dz}{z (1 + \alpha_{\text{NFW}} z)^2} = \ln \frac{(1 + \alpha_{\text{NFW}} r_{\epsilon_*})}{\alpha_{\text{NFW}} r_{\epsilon_*}} - \frac{1}{(1 + \alpha_{\text{NFW}} r_{\epsilon_*})}. \quad (\text{A4})$$

-
- [1] P. A. R. Ade *et al.* (Planck), *Astron. Astrophys.* **594**, A13 (2016), arXiv:1502.01589 [astro-ph.CO].
- [2] J. F. Navarro, C. S. Frenk, and S. D. M. White, *Astrophys. J.* **490**, 493 (1997), astro-ph/9611107.
- [3] A. Burkert, *The Astrophysical Journal Letters* **447**, L25 (1995).
- [4] A. V. Maccio, S. Paduroiu, D. Anderhalden, A. Schneider, and B. Moore, *Mon. Not. Roy. Astron. Soc.* **424**, 1105 (2012), arXiv:1202.1282 [astro-ph.CO].
- [5] W. J. G. de Blok, *Advances in Astronomy* **2010**, 14 pages (2010).
- [6] S.-H. Oh, W. J. G. de Blok, E. Brinks, F. Walter, and J. R. C. Kennicutt, *aj* **141**, 193 (2011), arXiv:1011.0899.
- [7] T. Sawala, Q. Guo, C. Scannapieco, A. Jenkins, and S. White, *MNRAS* **413**, 659 (2011), arXiv:1003.0671.
- [8] A. A. Klypin, A. V. Kravtsov, O. Valenzuela, and F. Prada, *Astrophys. J.* **522**, 82 (1999), arXiv:astro-ph/9901240 [astro-ph].
- [9] M. Boylan-Kolchin, J. S. Bullock, and M. Kaplinghat, *mnras* **415**, L40 (2011), arXiv:1103.0007 [astro-ph.CO].
- [10] J. S. Bullock and M. Boylan-Kolchin, *Ann. Rev. Astron. Astrophys.* **55**, 343 (2017), arXiv:1707.04256 [astro-ph.CO].
- [11] M. Kaplinghat, S. Tulin, and H.-B. Yu, *Phys. Rev. Lett.* **116**, 041302 (2016), arXiv:1508.03339 [astro-ph.CO].
- [12] A. Gonzalez-Samaniego, V. Avila-Reese, and P. Colin, *Astrophys. J.* **819**, 101 (2016), arXiv:1512.03538 [astro-ph.GA].
- [13] M. Drewes *et al.*, *JCAP* **1701**, 025 (2017), arXiv:1602.04816 [hep-ph].
- [14] T. Matos, F. S. Guzman, and L. A. Urena-Lopez, *Class.Quant.Grav.* **17**, 1707 (2000), arXiv:astro-ph/9908152 [astro-ph].
- [15] W. Hu, R. Barkana, and A. Gruzinov, *Physical Review Letters* **85**, 1158 (2000), astro-ph/0003365.
- [16] J. Goodman, *New Astronomy* **5**, 103 (2000), astro-ph/0003018.
- [17] T. Matos and L. A. Urena-Lopez, *Phys.Rev.* **D63**, 063506 (2001), arXiv:astro-ph/0006024 [astro-ph].
- [18] C. G. Böhrer and T. Harko, *Journal of Cosmology and Astroparticle Physics* **6**, 025 (2007), arXiv:0705.4158.
- [19] Schive Hsi-Yu, Chiueh Tzihong, and Broadhurst Tom, *Nat Phys* **10**, 496 (2014).
- [20] F.-Y. Cyr-Racine, K. Sigurdson, J. Zavala, T. Bringmann, M. Vogelsberger, and C. Frommer, *Phys. Rev.* **D93**, 123527 (2016), arXiv:1512.05344 [astro-ph.CO].
- [21] L. A. Ureña López and A. X. Gonzalez-Morales, *JCAP* **1607**, 048 (2016), arXiv:1511.08195 [astro-ph.CO].
- [22] R. Hlozek, D. Grin, D. J. E. Marsh, and P. G. Ferreira, *Phys. Rev.* **D91**, 103512 (2015), arXiv:1410.2896 [astro-ph.CO].
- [23] H.-Y. Schive and T. Chiueh, (2017), arXiv:1706.03723 [astro-ph.CO].
- [24] F. X. Linares Cedeño, A. X. Gonzalez-Morales, and L. Arturo Ureña López, (2017), arXiv:1703.10180 [gr-qc].
- [25] U.-H. Zhang and T. Chiueh, (2017), arXiv:1705.01439

- [astro-ph.CO].
- [26] U.-H. Zhang and T. Chiueh, Phys. Rev. **D96**, 023507 (2017), arXiv:1702.07065 [astro-ph.CO].
- [27] V. Iri, M. Viel, M. G. Haehnelt, J. S. Bolton, and G. D. Becker, (2017), arXiv:1703.04683 [astro-ph.CO].
- [28] E. Armengaud, N. Palanque-Delabrouille, D. J. E. Marsh, J. Baur, and C. Yche, (2017), arXiv:1703.09126 [astro-ph.CO].
- [29] T. Bernal, L. M. Fernández-Hernández, T. Matos, and M. A. Rodríguez-Meza, (2017), arXiv:1701.00912 [astro-ph.GA].
- [30] A. X. González-Morales, D. J. E. Marsh, J. Peñarrubia, and L. Ureña-López, (2016), arXiv:1609.05856 [astro-ph.CO].
- [31] S.-R. Chen, H.-Y. Schive, and T. Chiueh, (2016), arXiv:1606.09030 [astro-ph.GA].
- [32] H.-Y. Schive, M.-H. Liao, T.-P. Woo, S.-K. Wong, T. Chiueh, T. Broadhurst, and W.-Y. P. Hwang, Physical Review Letters **113**, 261302 (2014), arXiv:1407.7762.
- [33] R. Ruffini and S. Bonazzola, Phys. Rev. **187**, 1767 (1969).
- [34] F. S. Guzman and L. A. Urena-Lopez, Phys. Rev. **D69**, 124033 (2004), arXiv:gr-qc/0404014 [gr-qc].
- [35] A. X. González-Morales, A. Diez-Tejedor, L. A. Ureña-López, and O. Valenzuela, Phys. Rev. D **87**, 021301 (2013), arXiv:1211.6431 [astro-ph.CO].
- [36] A. Diez-Tejedor, A. X. Gonzalez-Morales, and S. Profumo, Phys. Rev. **D90**, 043517 (2014), arXiv:1404.1054 [astro-ph.GA].
- [37] R. Gavazzi, T. Treu, J. D. Rhodes, L. V. E. Koopmans, A. S. Bolton, S. Burles, R. J. Massey, and L. A. Moustakas, Astrophys. J. **667**, 176 (2007), astro-ph/0701589.
- [38] S. Mollerach and E. Roulet, *Gravitational lensing and microlensing by Silvia Mollerach, and Esteban Roulet. xi, 191 p. : ill. ; 23 cm. Includes bibliographical references and index. ISBN : 9810248520* (2002).
- [39] Y. Park and H. C. Ferguson, apjl **589**, L65 (2003), astro-ph/0304317.
- [40] C. O. Wright and T. G. Brainerd, apj **534**, 34 (2000).
- [41] D. J. E. Marsh and A.-R. Pop, ArXiv e-prints (2015), arXiv:1502.03456.
- [42] M. W. Auger, T. Treu, A. S. Bolton, R. Gavazzi, L. V. E. Koopmans, P. J. Marshall, K. Bundy, and L. A. Moustakas, Astrophys. J. **705**, 1099 (2009), arXiv:0911.2471.
- [43] L. Hui, J. P. Ostriker, S. Tremaine, and E. Witten, Phys. Rev. D **95**, 043541 (2017), arXiv:1610.08297 [astro-ph.CO].
- [44] S. Winitzki, “A handy approximation for the error function and its inverse,” (2008), available online at <http://sites.google.com/site/winitzki/sergeiwinitzkis-files/erf-approx.pdf>.
- [45] F. Feroz, M. P. Hobson, and M. Bridges, Mon. Not. Roy. Astron. Soc. **398**, 1601 (2009), arXiv:0809.3437 [astro-ph].
- [46] L. A. Ureña López, V. H. Robles, and T. Matos, (2017), arXiv:1702.05103 [astro-ph.CO].
- [47] B. Schwabe, J. C. Niemeyer, and J. F. Engels, Phys. Rev. **D94**, 043513 (2016), arXiv:1606.05151 [astro-ph.CO].
- [48] J. Veltmaat and J. C. Niemeyer, Phys. Rev. **D94**, 123523 (2016), arXiv:1608.00802 [astro-ph.CO].
- [49] P. Mocz, M. Vogelsberger, V. Robles, J. Zavala, M. Boylan-Kolchin, and L. Hernquist, (2017), arXiv:1705.05845 [astro-ph.CO].